ELSEVIER

Advances in Water Resources 24 (2001) 803–819

Advances in Water Resources

www.elsevier.com/locate/advwatres

Modeling unstable alcohol flooding of DNAPL-contaminated columns

Eberhard Roeder [a,*], Ronald W. Falta [a,b,1]

[a] Department of Geological Sciences, Clemson University, 340 Brackett Hall, Clemson, SC 29634-0976, USA
[b] Department of Environmental Engineering and Science, Clemson University, L.G. Rich Lab, Clemson, SC 29634-0919, USA

Received 12 November 1999; received in revised form 25 September 2000; accepted 27 October 2000

Abstract

Alcohol flooding, consisting of injection of a mixture of alcohol and water, is one source removal technology for dense non-aqueous phase liquids (DNAPLs) currently under investigation. An existing compositional multiphase flow simulator (UTCHEM) was adapted to accurately represent the equilibrium phase behavior of ternary and quaternary alcohol/DNAPL systems. Simulator predictions were compared to laboratory column experiments and the results are presented here. It was found that several experiments involved unstable displacements of the NAPL bank by the alcohol flood or of the alcohol flood by the following water flood. Unstable displacement led to additional mixing compared to ideal displacement. This mixing was approximated by a large dispersion in one-dimensional simulations and or by including permeability heterogeneities on a very small scale in three-dimensional simulations. Three-dimensional simulations provided the best match. Simulations of unstable displacements require either high-resolution grids, or need to consider the mixing of fluids in a different manner to capture the resulting effects on NAPL recovery.

Keywords: Alcohol flooding; Multicomponent; Compositional; DNAPL; Model; Displacement instability

1. Introduction

Alcohol flooding of DNAPL contamination is under investigation as a remediation technology (e.g. [23,26,43]). Numerical models can play an important role in understanding and designing experiments involving the complex phase behavior, and eventually will be necessary to design field remediation schemes. The objective of the work reported here was to validate a simulator for alcohol flooding by comparison to a set of vertical column experiments [9,10,44]. Particular emphasis was placed on the matching of unstable displacements.

Two recent modeling studies of alcohol flooding focused on the overriding properties of the flooding solution over the resident water and did not consider NAPL–alcohol interactions [29,33]. Previously, Brame [8] extended the capabilities of a three-dimensional integral finite difference multiphase simulator to a three-component system for alcohol flooding, and compared simulation results to results from column experiments. Reitsma [52–55] developed a one-dimensional finite element simulator for two-phase, three-component flow, and simulated some of the same experiments as Brame [8]. In both of these simulation studies did the models overpredict DNAPL mobilization during mobilizing alcohol floods.

Enhanced petroleum recovery involves processes similar to NAPL remediation [24,59]. One petroleum engineering simulator that has been adapted to environmental use is the University of Texas Chemical Flooding simulator (UTCHEM) [11,12,18,33,47]. Its incorporation of a numerical dispersion control and the modeling of up to five volume-occupying components made it an attractive candidate for modification and application to alcohol flooding. The adaptation of this simulator to the phase behavior occurring in alcohol flooding is described in more detail elsewhere [57].

Three column experiments, one enhanced-dissolution, two mobilization, were chosen for simulation: (1) The ternary system iso-propanol (IPA)–tetrachloroethene (PCE)–water [4,9,10] as one in which the alcohol mainly enhances the solubility of NAPL component in

* Corresponding author.
E-mail addresses: eberhard_roeder@hotmail.com (E. Roeder), faltar@clemson.edu (R.W. Falta).
[1] Tel.: +1-864-656-1025; Fax: +1 864-656-1041.

0309-1708/01/$ - see front matter
PII: S0309-1708(00)00072-5

Nomenclature

a	dispersivity (m)
A_l	solubility parameter for phase l in Hand-representation
B_l	solubility parameter for phase l in Hand-representation
$B_{l,0}$	solubility parameter for phase l in the absence of additive
C_l^i	volume fraction of component i in phase l (v/v)
C^i	total concentration of i, sum of component i in all phases l (v/v)
C_{pl}^n	concentration of NAPL component at plait point (v/v)
$C_{pl,0}^n$	concentration of NAPL component at plait point without additive (v/v)
$C_{max'}^c$	equivalent height of solubility curve (v/v)
C_{min}^c	concentration of alcohol at which Hand-representation begins to be used (v/v)
C_p^c	concentration of alcohol in the cosolvent-poor phase (v/v)
C_{pc}	capillary pressure parameter intrinsic to the medium (kPa m)
d_{ij}	binary interaction parameter for volume-based [27] viscosity function
g	gravity (m/s^2)
E	plait point parameter for tie-line description in Hand-representation
F	tie-line parameter for tie-line description in Hand-representation
f_w^a	fraction of additive in aqueous pseudo-component: $f_w^a = C^a/(C^a + C^w)$ (v/v)
i, j	component indices (water ($i = w$); NAPL component ($i = n$); cosolvent ($i = c$); additive ($i = a$))
k	intrinsic permeability of the medium (m^2)
k_{rl}	saturation dependent relative permeability for phase l
k_{rl0}	relative permeability to phase l at residual saturation of the other phase
k_{rl0}^{low}	relative permeability to phase l at residual saturation of the other phase at low trapping number
k_{rl0}^{high}	relative permeability to phase l at residual saturation of the other phase at high trapping number
$k_{Li\ and\ Fu}$	exponent for interfacial tension function
$k_{Li\ and\ Fu,0}$	exponent for interfacial tension function in the absence of additive
l	phase index (aqueous ($l = w$); NAPL ($l = n$))
n	model parameter for van Genuchten capillary pressure function: $m = 1 - 1/n$
N_{Tl}	trapping number for phase l
P_l	pressure of phase l (Pa)
P_c	capillary pressure of phase l (Pa)
S_l	saturation of the liquid phase l (v/v)
S_e	effective aqueous saturation: $(S_e = (S_w - S_{rw})/(1 - S_{rw} - S_{rn})$ if residual NAPL is present
S_{rl}	residual saturation of phase l (v/v)
S_{rl}^{low}	residual saturation of phase l (v/v) at low trapping number
S_{rl}^{high}	residual saturation of phase l (v/v) at high trapping number
Sol	solubility of NAPL component in the aqueous phase at low alcohol concentrations (v/v)
Sol_0	Sol in absence of additive (v/v)
T_l	desaturation parameter for phase l. Set $T_w = 10{,}000$; $T_n = 1000$
v_{crit}	initial Darcy flux that distinguishes stable from unstable disagreement
x'_{ij}	fraction of the indicator component in the binary mixture: $x'_{ij} = C^i/(C^i + C^j)$. i is the alcohol (or additive) in mixtures of alcohol (or additives) with water or NAPL component
$x_{ij\,max}$	fraction of the component i in a binary mixture with j at which density deviation is maximum (0.5 in the cases under consideration here)
X	mutual solubility term: $X = \log(C_n^w + C_w^n + C_p^c)$
X_0	mutual solubility term in absence of alcohol
$X_{0,0}$	mutual solubility term in absence of alcohol and additive

Greek symbols

α	model parameter for van Genuchten capillary pressure function related to entry pressure (1/kPa)
α_l	influence of additive on slope parameter of solubility curve for phase l
β	angle between direction of flow and the horizontal (positive upward)
ϵ_l	exponent for Brooks and Corey relative permeability function.
ϵ_l^{low}	exponent for relative permeability function at low trapping number. Here set $\epsilon_w = \epsilon_n = (2 + 3\lambda)/\lambda$
ϵ_l^{high}	exponent for relative permeability function at high trapping number: set $\epsilon_w = \epsilon_n = 1$
ϕ	porosity (dimensionless)
Φ_l	potential of fluid 1

θ	angle between local flow direction and the horizontal (counter clockwise)	ρ_l	density of phase l (g/ml)
λ	pore distribution index	$\Delta\rho_{i,j}$	adjustment to density of component i in a binary mixture with component j to account for nonideal mixing (g/ml)
μ_l	composition dependent viscosity (cP = mPa s)	σ	interfacial tension between NAPL and aqueous phases (dynes/cm = mN/m)
$\rho_{i,0}$	reference density of component i (g/ml)	σ_0	interfacial tension between pure NAPL component and water (mN/m)
$\rho_{i,l}$	density of component i in phase l (g/ml)		

the aqueous phase; (2) The ternary system tert-butanol (TBA)–PCE–water [9,10] as an example of systems in which the alcohol swells the NAPL phase; and (3) the NAPL-swelling quaternary system, *n*-butanol–trichloroethene (TCE)–water–methanol [44]. Methanol in this quaternary system was added for the purpose of enhancing the solubility of *n*-butanol in water and affected all aspects of phase behavior. Cases (1) and (2) had been simulated in one-dimensional simulations before [8,52,55]. The experiments used the same glass bead medium throughout.

2. Displacement instability

Displacement instability occurs if the displacing fluid experiences less resistance to flow than the displaced fluid at a perturbed interface. It is caused by density and viscosity contrasts between the two fluids. In a stable displacement, small perturbations in the displacement front will not expand. This criterion can be used to derive a critical Darcy flux, v_{crit}, that distinguishes stable from unstable miscible displacement for a fluid, indexed 1, displacing a second fluid, indexed 2 [7,34,35,59]:

$$v_{crit} = \frac{kk_{r1}\Delta\rho g \sin\beta}{\mu_1(M-1)} = \frac{kk_{r1}(\rho_1-\rho_2)g\sin\beta}{\mu_1(k_{r1}\mu_2/k_{r2}\mu_1-1)}. \quad (1)$$

The notation is explained in the Nomenclature. A gravity term in the numerator greater than zero indicates that the less dense fluid is on top, a stable situation. A mobility ratio, M, of less than one, resulting in a negative denominator, indicates that the less mobile liquid displaces the more mobile one, which also signifies a stable displacement. The critical displacement flux can therefore be larger than zero only if gravity or viscous stability exists to balance a viscous or gravity instability, respectively. Displacements involving a viscous instability are stable up to the critical flux, displacements involving a gravity instability are stable beyond the critical flux. If both viscous and gravity stability is present then the displacement is unconditionally stable. If neither stability is present then the displacement is always unstable. In either of these two cases no critical flux exists and the negative numerical value obtained from Eq. (1) is meaningless.

Dispersion, boundary effects [16,35,66], and capillary pressure have a stabilizing effect on unstable displacements. For low interfacial tensions or in the absence of interfacial tensions, as expected during miscible displacements, and medium to highly permeable material as under consideration here, the stabilizing influence of capillary pressure is negligible [31,65], and the stability analysis developed for single-phase flow is applicable.

Unstable displacements cause an expansion of perturbations in the displacement front. This fingering results in apparent dispersion when concentrations are averaged across fingers of displacing fluid and remainders of displaced fluid [35,50,59]. If a breakthrough of the displacing fluid occurs because such a finger has reached the extraction point, the subsequent flow of displacing fluid occurs mainly via this channel and recovery of the fluid that was to be displaced is drastically reduced [3,35].

Simulations of unstable displacements take generally one of two approaches. One approach considers only one-dimensional flow and includes the non-ideal displacement that occurs due to instability or heterogeneity of the medium as a mixing term akin to dispersion [35,50]. This approach has led to analytical approximations which indicate that the apparent dispersion is time dependent [60,66]. Matching effluent concentrations with numerical simulations is one possibility to obtain the apparent dispersion coefficient of a porous medium for a given time and position. This value cannot readily be used to predict the mixing at a different location and time during an unstable displacement. For very unstable displacements, the resulting fingering results in breakthrough curves that can not be approximated by a dispersion term [3,37]. The other approach represents the fingering more directly by using a fine numerical grid in usually two [45,50,61] and less commonly three [13] dimensions of flow. This approach is computationally far more intensive, but allows observation of finger growth over time. One practical limitation of this second approach is the spatial resolution required for representation of the fingers. The analysis by Tan and Homsy [60] suggests that fingers during unstable displacement develop at a distance from each other that is an order of magnitude smaller than the longitudinal dispersivity. For homogeneous media, this

spatial resolution may be impracticable. But because only some of the initial fingers continue to grow and eventually dominate the displacement pattern [45], a coarser grid resolution should still represent most of the fingering phenomenon accurately.

In the present study, both approaches were used. The simulator used here had an adjustable dispersivity to allow distinction between the dispersivity of the medium and mixing effects due to unstable displacement in one-dimensional simulations. Three-dimensional simulations with a resolution sufficient to represent the influence of heterogeneities on stable displacements were performed to represent the fingering effects during unstable displacement more directly.

3. General description of simulator

UTCHEM is a three-dimensional, multiphase, multicomponent simulator that has been adapted to environmental use from its origin in enhanced oil recovery [11,12,18,33,47]. The simulator can incorporate a multitude of components, the most important of which for the purposes of the present study were water, NAPL component, primary alcohol, additive (secondary alcohol), and tracers. UTCHEM utilizes a solution scheme that is implicit in pressure and explicit in concentrations (IMPESC-like). A total variation diminishing scheme with third-order spatial discretization is used to control numerical dispersion [17,30,40].

The version used for this work was UTCHEM 5.32 m and was obtained from the University of Texas [18]. Its equilibrium phase property descriptions were modified to accurately describe the phase behavior for DNAPL component, alcohol, water systems [57]. The relationships used for the description of medium and phase properties are discussed briefly below.

UTCHEM uses a pseudocomponent approach [49,58] to reduce to three the number of active agents for phase partitioning purposes. The partitioning behavior of these three components, primary alcohol, NAPL component and water, between two phases is modeled based on the Hand representation [28,62]. Brandes [9,10] observed some cloudy samples in his experiments. Milazzo [44] found only two phases in his experiments. Emulsions were not considered as a third phase in the present simulations, equivalent to assuming that the observed cloudiness was caused by insufficient separation times of suspended NAPL in the sample and not by stable emulsions.

The Hand representation is based on a plot of concentration ratios on a log–log scale (Table 1). The solubility curve and lines of equal phase composition (tie-lines) are represented by straight lines on such a plot. The plait point is the point on the solubility curve where both phase compositions are equal, so that the lines of the solubility curve and the tie-lines intersect. In the Hand representation, concentrations of NAPL component in the aqueous phase at low alcohol concentrations are much smaller than the true aqueous solubility. In UTCHEM, a minimum alcohol concentration, C^{c}_{min}, is used at which phase composition calculations change to the Hand representation from a model where all alcohol is associated with the water, and NAPL-component solubility is given as input parameter.

Table 1
Relationships used to describe phase compositions in the presented version of UTCHEM

Solubility curve	$\frac{C^{c}_{l}}{C^{n}_{l}} = A_l \left(\frac{C^{c}_{l}}{C^{w}_{l}} \right)^{B_l}$
Equivalent height of the solubility curve	$C^{c}_{max'} = \frac{\sqrt{A_l}}{\sqrt{A_l}+2}$
Tie-line relationship	$\frac{C^{c}_{n}}{C^{n}_{n}} = E \left(\frac{C^{c}_{w}}{C^{w}_{w}} \right)^{F}$
Plait point parameter	$E = \frac{C^{c}_{pl}}{C^{n}_{pl}} \left(\frac{C^{c}_{pl}}{C^{w}_{pl}} \right)^{-F}$
Solubility curve parameter A_l change with additive	$\log A_l = \log A_{l,0} + f^{a}_{w} \frac{\Delta \log A_l}{\Delta f^{a}_{w}}$
Solubility curve parameter B_l change with additive	$B_l = B_{l,0} + \exp\left(\alpha_l f^{a}_{w}\right)$
Solubility (for $C^{c} < C^{c}_{min}$)	$\log \mathrm{Sol} = \log \mathrm{Sol}_0 + f^{a}_{w} \frac{\Delta X_0}{\Delta f^{a}_{w}}$
Tie-line parameter change	$F = F_0 + f^{a}_{w} \frac{\Delta F}{\Delta f^{a}_{w}}$
Plait point location change	$\frac{1}{C^{n}_{pl}} = \frac{1}{C^{n}_{pl,0}} + f^{a}_{w} \frac{\Delta(1/C^{n}_{pl})}{\Delta f^{a}_{w}}$

The fourth component added to the ternary system primary alcohol–NAPL component–water is distributed in the model between the three other components, resulting in three pseudocomponents [49,57,58]. In the quaternary system under consideration in the present work, the fourth component methanol had a strong tendency to associate with the water. Therefore, the water pseudocomponent was assumed to be a mixture of water and methanol. Changing the composition of the water pseudocomponent changes the partitioning behavior of the primary alcohol and the mutual solubilities of NAPL component and water pseudocomponent. The data by Milazzo [44] for the water–TCE–*n*-butanol–methanol quaternary system were used to define the forms of relationships between methanol concentration added to water and pseudoternary behavior [57], which are shown in Table 1.

Phase properties were modeled in the following manner (Table 2). For phase viscosities, a volume-based approach using binary interaction parameters [27,51] was found to match data for multicomponent mixtures including water [57]. The density of a phase was calcu-

Table 2
Relationships for phase properties in the presented version of UTCHEM

Interfacial tension (mN/m)	$\sigma = \sigma_0 \left(\frac{X}{X_0}\right)^{k_{\text{Li and Fu}}}$
Interfacial tension exponent	$k_{\text{Li and Fu}} = k_{\text{Li and Fu},0} + f_{\text{w}}^{\text{a}} \frac{\Delta k_{\text{Li and Fu}}}{\Delta f_{\text{w}}^{\text{a}}}$
Interfacial tension mutual solubility term	$X_0 = X_{0,0} + f_{\text{w}}^{\text{a}} \frac{\Delta X_0}{\Delta f_{\text{w}}^{\text{a}}}$
Viscosity of phase l (mPa s)	$\ln \mu_{\text{l}} = \sum_i C^i \ln \mu_i + \sum_i \sum_{j>i} C^i C^j d_{i,j}$
Density of phase l (g/ml)	$\rho_{\text{l}} = \sum_i C_{\text{l}}^i \left(\rho_{i,0} + \sum_{j \neq i} \Delta\rho_{i,j} - \frac{\Delta\rho_{i,j}}{x_{ij\max}^2} (x'_{ij} - x_{ij\max})^2 \right)$

lated as volume-weighted average of the component densities at the experimental temperature [51]. To account for non-ideal mixing, the individual component densities were adjusted as a function of composition [57]. A volume-based correlation for the interfacial tension modified from one proposed by Li and Fu [38] was implemented, in which the interfacial tension is a function of the interfacial tension in the absence of alcohol and a power term reflecting the influence of the alcohol [57].

Medium properties were represented as summarized in Table 3. Capillary pressures were modeled using the relationship proposed by van Genuchten [63] and Corey-type functions were used for the relative permeability [18]. Residual saturations varied as a function of the total trapping number [18,46]. Dispersivity was assumed to be constant for each run. For all runs, the transverse dispersivity was set to one third of the longitudinal dispersivity [19]. Molecular diffusion was small compared to convective dispersion and therefore not considered separately.

4. Column experiments

The column experiments discussed here were performed and described by Brandes [9,10] and Milazzo [44]. A schematic of their experimental set-up is shown in Fig. 1. Glass columns with an inside diameter of 2.5 cm were used. The porous medium consisted of equal weight fractions of 0.1, 0.3, and 0.5 mm glass beads. The glass beads were packed wet in layers of approximately three centimeters. Packing length was approximately 60 cm. Adjustable plungers kept the glass beads in place. In the experiments by Brandes [9,10], filter discs were used in the plungers to keep glass beads out of the tubing. Milazzo [44] replaced the filter disc on the effluent side with glass wool and shortened the effluent tubing.

Brandes [9,10] determined the porosity and pore volume of packed columns by the bulk density of the packed volume and the density of the medium. The resulting pore volumes then did not account for influent and effluent tubing. Milazzo [44] packed the column in the same way and performed a tracer test to determine effective pore volume. This tracer experiment also provided information on the dispersivity of the medium as discussed below.

Brandes [9,10] emplaced the NAPL in his experiments by injecting 1.5 PV of NAPL (TCE or PCE) downwards into the column. The NAPL was then displaced in downward direction by three pore volumes of water. Milazzo [44] introduced the contaminant (TCE) in upward direction to fill two fifths of the column length. The NAPL was displaced in downward direction as done by Brandes [9,10]. The column was then turned for the NAPL contamination to be at the top.

Alcohol flooding consisted of injection of approximately one pore volume of flooding solution into the lower end of the column, followed by approximately three pore volumes of water in the same direction. Milazzo [44] used a peristaltic pump to achieve a constant flow rate, while Brandes [9,10] gave a constant gradient of 0.3. This constant gradient was interpreted

Table 3
Relationships used to describe porous medium properties in UTCHEM

Capillary pressure (kPa)	$P_{\text{c}} = \frac{1}{\alpha}\left(\frac{1}{S_{\text{e}}^{1/m}} - 1\right)^{1/n} = C_{\text{pc}} \sqrt{\frac{\phi}{k}} \frac{\sigma}{\sigma_0} \left(\frac{1}{S_{\text{e}}^{1/m}} - 1\right)^{1/n}$
Relative permeability	$k_{\text{rw}} = k_{\text{rw0}} (S_{\text{e}})^{\varepsilon_{\text{w}}}; k_{\text{rn}} = k_{\text{rn0}} (1 - S_{\text{e}})^{\varepsilon_{\text{n}}}$
Trapping influence on residual saturation	$S_{\text{rl}} = \min\left(S_{\text{l}}, S_{\text{rl}}^{\text{high}} + \frac{S_{\text{rl}}^{\text{low}} - S_{\text{rl}}^{\text{high}}}{1 + T_{\text{l}} N_{\text{Tl}}}\right)$
Trapping number for fluid 2 displaced by fluid 1 [18]	$N_{T2} = \frac{k}{\sigma} \sqrt{(-\lvert\nabla\Phi_{\text{l}}\rvert)^2 + 2(-\lvert\nabla\Phi_{\text{l}}\rvert) g(\rho_2 - \rho_1) \sin\theta + (g(\rho_2 - \rho_1))^2}$
Influence of decreasing residual saturation on relative permeability	$k_{\text{rl0}} = k_{\text{rl0}}^{\text{low}} + \frac{S_{\text{rl}}^{\text{low}} - S_{\text{rl}}}{S_{\text{rl}}^{\text{low}} - S_{\text{rl}}^{\text{high}}} \left(k_{\text{rl0}}^{\text{high}} - k_{\text{rl0}}^{\text{low}}\right)$
	$\varepsilon_{\text{l}} = \varepsilon_{\text{l}}^{\text{low}} + \frac{S_{\text{rl}}^{\text{low}} - S_{\text{rl}}}{S_{\text{rl}}^{\text{low}} - S_{\text{rl}}^{\text{high}}} \left(\varepsilon_{\text{l}}^{\text{high}} - \varepsilon_{\text{l}}^{\text{low}}\right)$

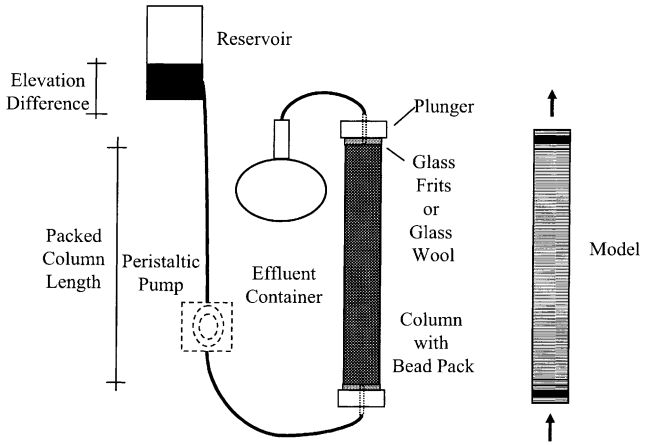

Fig. 1. Experimental set-up used by Brandes [9,10] and Milazzo [44]. Brandes used an elevation gradient to drive the flow, Milazzo used a peristaltic pump.

in the present work as initial elevation gradient $(\Delta z/\Delta L)$ because the influence of composition on injection fluid densities was not considered [9,10]. In previous simulations of Brandes' [9,10] experiments, Brame [8] attempted to match the flow rates given by Brandes [9,10] for a constant gradient but used the given flow rates as driving force for the reported simulations. Reitsma [52,55] apparently applied constant head boundary conditions to the simulated columns and did not address the issue of flow rates.

5. Application of the simulator to vertical column experiments

The approach taken for the simulation of the column experiments consisted of the following. First, the dispersivity of the medium was matched based on the results of a conservative tracer experiment by Milazzo [44]. Subsequently, an enhanced dissolution experiment (PCE/IPA) by Brandes [9,10] was simulated to investigate a case where the NAPL phase would not be mobilized. Then, separate phase mobilization cases (PCE/TBA) by Brandes [9,10] and (TCE/*n*-butanol/methanol) by Milazzo [44] were simulated. Agreement between experiments and simulations was determined visually by plotting and comparison of effluent concentrations and effluent volumes.

One-dimensional and three-dimensional representations of the columns were considered. Brame [8] and Reitsma [52,55] used one-dimensional homogeneous medium equivalents of the experimental columns. The one-dimensional representation discussed in the following accounted for the influence of the filter discs, which Milazzo [44] found to be significant with respect to permeability. The heterogeneous three-dimensional representations of the column included the influence of the filter discs in the same manner as the one-dimensional ones.

5.1. Column model parameters

The discretization of the column consisted lengthwise of 150 gridblocks of 0.44 cm length each. Of these, the top and bottom five layers represented a porous medium equivalent of effluent and influent apparatus, respectively. The glass filter discs were assumed to be at the center of these five sections. The three-dimensional model discussed here represented the column cross section with five by five approximately cubical gridblocks, which resulted in run times on the order of a week for mobilization simulations. It was assumed that the difference in shape did not impact simulation results. In all simulations, a uniform porosity of 0.33 and a total pore volume of 107 ml were assumed [44]. Table 4 lists the porous medium properties in the column discretizations.

Fluids were injected in the center of the bottom-most layer, and extracted in the center of the uppermost layer. If constant gradient conditions were specified as in Brandes' [9,10] experiments, the injection pressure differentials were estimated from the density of the injected solution, the length of the modeled column (66 cm), and the given gradient. For constant flow rate experiments as performed by Milazzo [44], the given flow rates were used. The outlet pressure was set to atmospheric (101 kPa) in all cases.

To obtain van Genuchten parameters for capillary pressure curves [63] from entry capillary pressure and pore size distribution parameter, the relationships by Lenhard et al. [36] were used. In UTCHEM, capillary pressures scale with the inverse of the square root of permeability [18]. Entry capillary pressure for the bead pack was estimated from the data for drainage of water against benzene measured by Boyd [6] for the 0.5 mm size fraction of the beads and adjusted for the difference in interfacial tensions between the NAPL/water pairs. These data were the only measured ones available for the medium used in the experiments. The pore size distribution parameter λ was set to two [15], which accounted for the wider pore size distribution in the glass bead mix compared to the 0.5 mm size fraction. The filter discs used were 1.9 cm diameter glass filter discs classified as porosity C [1]. The porosity classification is based on the entry pressure for a nonwetting phase [1]. An entry pressure between 6.4 and 3.2 kPa is expected for class C filter discs and an interfacial tension of 40 dynes/cm. The same distribution index, λ, as for glass beads was assumed.

Permeability of the column was estimated based on experiments by Brandes [9,10] and Milazzo [44]. Brandes [9,10] reported a permeability of 10 Darcy as result of permeability tests performed with influent and effluent filter discs. A reanalysis of flow data without

Table 4
Porous medium properties for simulations of glass bead experiments

Parameter	One-dimensional column with filter discs	Three-dimensional column
Dimensions in z	150×0.0044 m	150×0.0044 m
Dimensions in x, y	0.0222 m $\times 0.0222$ m	5×0.00443 m $\times 5 \times 0.00443$ m
Porosity	0. 33[a]	0. 33[a]
Bead pack van Genuchten capillary pressure parameters	$\alpha = 1.75$ 1/kPa(PCE/water)[b]	$\alpha = 1.75$ 1/kPa(PCE/water)[b]
	$\alpha = 1.63$ 1/kPa(TCE/water)[b]	$\alpha = 1.63$ 1/kPa(TCE/water)[b]
	$m = 0.77$[c]	$m = 0.77$[c]
Filter discs capillary pressure parameters	$\alpha = 0.15$ 1/kPa[d]	$\alpha = 0.15$ 1/kPa[d]
	$m = 0.77$[c]	$m = 0.77$[c]
Effective permeability of column setup	$k = 10 \times 10^{-12}$ m^2[a]	$k = 10 \times 10^{-12}$ m^2[a]
	$k = 4.2 \times 10^{-12}$ m^2[e]	$k = 4.2 \times 10^{-12}$ m^2[e]
Permeability of pack	$k = 18.4 \times 10^{-12}$ m^2[e]	$k_{\text{average}} = 18.4 \times 10^{-12}$ m^2[e]
Relative permeability	$k_{\text{rw0}}^{\text{low}} = 0.46$	$k_{\text{rw0}}^{\text{low}} = 0.46$
	$k_{\text{rn0}}^{\text{low}} = 0.46$[c]	$k_{\text{rn0}}^{\text{low}} = 0.46$[c]
	$\epsilon^{\text{low}} = 4$[c]	$\epsilon^{\text{low}} = 4$[c]
	$\epsilon^{\text{high}} = 1$	$\epsilon^{\text{high}} = 1$
Residual saturation	$S_{\text{rw}}^{\text{low}} = 0.16$[b]	$S_{\text{rw}}^{\text{low}} = 0.16$[b]
	$S_{\text{rn}}^{\text{low}} = 0.16$[a]	$S_{\text{rn}}^{\text{low}} = 0.16$[a]
	$S_{\text{rn}}^{\text{low}} = 0.05$[e]	$S_{\text{rn}}^{\text{low}} = 0.05$[e]
Desaturation parameter	$T_{\text{n}} = 10{,}000$	$T_{\text{n}} = 10{,}000$
	$T_{\text{w}} = 1000$	$T_{\text{w}} = 1000$

[a] From Brandes [9,10].
[b] Based on data from Boyd [6].
[c] Estimate using $\lambda = 2$ in Brooks–Corey relationship.
[d] Based on Ace Glass [1].
[e] Based on data from Milazzo [44].

top filter disc given by Milazzo [44] yielded a permeability of 4.2 Darcy. After removing the bottom filter disc, Milazzo [44] repeated the permeability test for the same column from which a permeability of 18.4 Darcy was obtained. Therefore, the bead packing was assumed to have a permeability of 18.4 Darcy. To obtain the measured effective permeabilities of the column the influent and effluent section permeabilities were varied. The layer representing the filter disc was assigned the lowest permeability and the permeability of the adjacent layers was increased by a factor, so that the ratio of permeabilities of neighboring layers was constant from the last bead pack layer to the filter disc.

Brandes [9,10] measured the relative permeability for water after achieving residual saturation for the NAPL phase as 0.46. This is a fairly high value indicative of only slightly water wet glass beads [35]. Therefore, and in the absence of other data, the same relative permeability endpoint and exponent was used for all phases. The exponent ϵ in the relative permeability functions was estimated from the pore size distribution index using the Brooks–Corey relationship $\epsilon = (2 + 3\lambda)/\lambda$ [15]. This yielded an exponent of four, which was used for low trapping numbers [18,46], that is, ratios of gravity and viscous forces to capillary forces (Table 3). For high trapping numbers an exponent of one, equivalent to a linear dependence of relative permeability on saturation, was assumed [2,4].

Brandes [9,10] obtained experimentally a residual NAPL saturation of 16 ± 0.02 upon downward infiltration. Effluent concentrations and recovery reported by Milazzo [44] were converted into a NAPL volume. This yielded a residual saturation of approximately 0.05 for his experiment 2 and a residual saturation of 0.2 in his experiment 4. Milazzo [44] did not comment on this discrepancy. For simulations of his experiment 2, the measured residual NAPL saturation of 0.05 was used. The residual saturation of water was set equal to 0.16, which is in agreement with experiments by Boyd [6] and by Imhoff et al. [32] with similar media.

5.2. Dispersivity

The conservative tracer test performed by Milazzo [44] was used to determine the dispersivity of the medium. The point on the breakthrough curve where the normalized concentration measure was 0.5 was taken to be the pore volume (107 ml). The curve was then matched using the implementation [20] of an analytical solution for one-dimensional tracer advection under the influence of dispersion [64].

Overall, a dispersivity of about 0.06 cm described the breakthrough curve well (Fig. 2). The initial part of the breakthrough curve was steeper than the latter part. This indicates a small influence of dead-end pores or capacitance [14,35]. The numerical dispersivity of the column models was determined by simulating the tracer

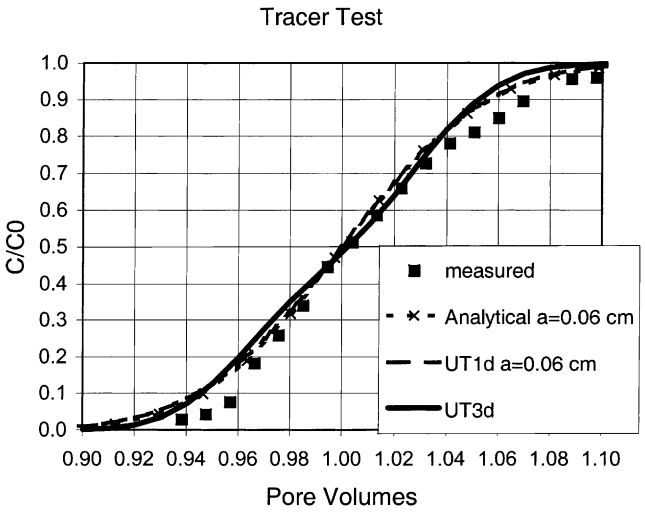

Fig. 2. Measured conductivity breakthrough curve [44], and dispersivity matches with an analytical solution and one-dimensional and three-dimensional UTCHEM models (UT1d and UT3d, respectively).

test with zero input dispersivity. Matches with the analytical solution indicated a value of 0.01 cm for the one- and three-dimensional models. This was negligible compared to the dispersion observed in the tracer experiment and an input dispersivity of 0.06 cm was used to match the measured tracer breakthrough curve with the numerical simulator (Fig. 2).

In previous simulations of the column experiments by Brandes [9,10], the numerical dispersion was between one and two orders of magnitude higher. Reitsma [52,55] set the cell length to 0.625 cm for which he obtained a numerical dispersivity of 1 cm. Brame [8] set the cell length to 0.6 cm and did not provide a dispersivity which, for upstream weighting, would be expected to be half the cell length or 0.3 cm.

To generate a three-dimensional heterogeneous model domain, the relationship between macrodispersivity and heterogeneity developed by Gelhar and Axness [25] was used. The packing lift height of 3 cm and column diameter of 2.5 cm were used as correlation lengths. Two conductivity fields for the packing length were realized using simulated annealing [22]. Because the results were very similar for both realizations throughout the simulations, only results from one realization are shown in the following. The gridblock permeabilities ranged from 10 to 31 darcy. Effluent and influent ends of the column remained homogeneous layers. The three-dimensional heterogeneous columns were used to simulate the tracer test with zero input dispersivity and matched the analytical solution and experimental data reasonably well (Fig. 2). Thus, a one-dimensional and a three-dimensional representation of the columns were available which matched the tracer test results by Milazzo [44].

5.3. Enhanced dissolution

Transfer of NAPL component from the NAPL into the aqueous phase characterizes NAPL remediation by dissolution. Increased NAPL solubility in the aqueous phase due to alcohol or surfactant addition enhances dissolution. Little NAPL movement occurs and therefore, relative permeability functions are of little importance. Among the experiments that have addressed enhanced dissolution, flushing of residual PCE with an IPA/water mixture as reported by Brandes [9,10] was selected. The given effluent concentrations in mg/l [9] were converted to volume fractions using the component densities. The phase behavior parameters of this system as determined from data by Bergelin et al. [5] are listed in Table 5.

In the experiment, 0.935 PV of a 60% IPA, 40% water mixture was injected into a column at residual PCE saturation under an elevation gradient given as 0.3. The alcohol flood was followed with 2.5 pore volumes of water flood in the same upward direction. The experimental data have been utilized in previous applications of alcohol flooding simulators [8,52,55].

In the simulations of the experiment discussed here, the match of cumulative volumes extracted was improved by changing the elevation gradient during the alcohol slug injection. Effluent concentrations were matched by changing dispersivities in one-dimensional simulations.

The simulated and measured cumulative pore volumes extracted during the experiment are compared in Fig. 3. A one-dimensional simulation with the given constant elevation gradient of 0.3 showed faster flows than were measured. A reduction in the gradient to

Table 5
Fluid properties for the IPA/PCE/water ternary system used in the simulation

$T = 23°C$	
Hand parameters for phase behavior [5,57]	C_{pl}^{n}: 0.492 (v/v)
	$B_n = B_w$: −1.71
	F: 1.07
C_{min}^{c}: 0.09	$C_{max'}^{c}$: 0.688 (v/v)
Interfacial tension [5,57]	σ_0: 40 mN/m
X_0: −3.6	$k_{Li\ and\ Fu}$: 2.88
Density (g/ml) [39,56]	Density adjustments [5,39,57]
	$\Delta\rho_{w,IPA}$: 0.031
ρ_w: 0.998	$\Delta\rho_{IPA,w}$: 0.026
ρ_{PCE}: 1.62	$\Delta\rho_{PCE,IPA}$: −0.006
ρ_{IPA}: 0.783	$\Delta\rho_{IPA,PCE}$: 0.001
Viscosity (mPa s) [39,56]	Interaction parameters [5,57]
μ_w: 0.95	$d_{w,PCE}$: 7.78
μ_{PCE}: 0.87	$d_{w,IPA}$: 3.21
μ_{IPA}: 2.16	$d_{PCE,IPA}$: −0.785

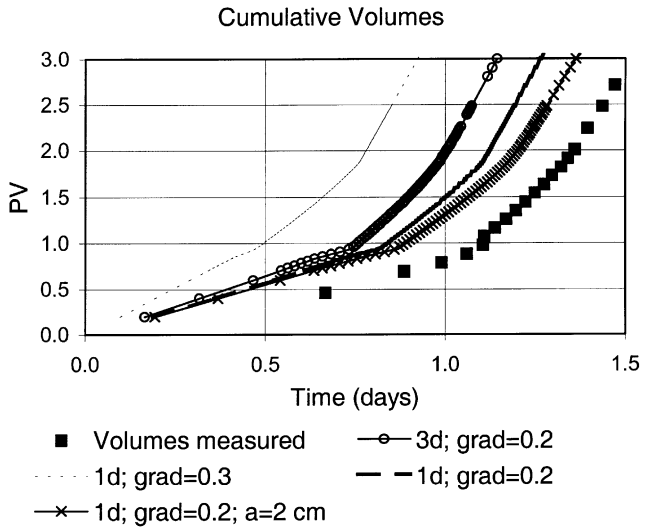

Fig. 3. Measured [9] and simulated cumulative pore volumes over time for 60% IPA flood with varying elevation gradient and dispersivity.

between 0.15 and 0.2 during the alcohol flood yielded a better agreement. The step in cumulative pore volumes at 1.1 days, which was not seen in the simulation, is likely related to the switching from an alcohol mixture to the water flood. A one-dimensional simulation with increased dispersivity ($a = 2$ cm) resulted in slower flow caused by the increased viscosity of water/alcohol mixtures before and after the core of the alcohol slug. The three-dimensional simulations showed an increase in flow rates compared to the one-dimensional simulations (Fig. 3). This was partially due to a higher effective permeability as also seen in the tracer simulations and partially due to preferential dissolution of some areas as also seen experimentally by Imhoff et al. [32].

The effluent concentrations in (v/v) for experimental results and simulations are shown in Fig. 4. The results from the one-dimensional model with medium dispersivity ($a = 0.06$ cm) are similar to the concentrations simulated by Brame [8] and Reitsma [52,55] for the same case. The simulated breakthroughs of elevated IPA and PCE concentration occurred simultaneously and agreed well with experimental results. The plateau concentrations of PCE and IPA were well matched, although PCE concentrations were lower in the simulations than measured (6.2% vs. 6.6% by volume). The same was the case for the IPA concentration (57% simulated, 60% measured by volume). Half of the difference could be attributed to volume reduction of alcohol/water mixtures, which was not considered during the effluent concentration conversion.

The primary contrast between the simulation ($a = 0.06$ cm) and experimental observations occurred during the transition to the water flood. The simulation predicted a sharp drop of IPA and PCE concentrations. In the experiment, the tailing of concentrations began before the end of the alcohol slug and continued through the end of the experiment. A one-dimensional simulation with a dispersivity of $a = 2$ cm replicated the tailing of the alcohol concentration better, but resulted in lower PCE concentrations and a premature breakthrough of IPA (Fig. 4).

Displacement instability was the likely cause for this tailing effect. The displacement of resident water by PCE–saturated IPA solution was stable, while the displacement of PCE–saturated IPA solution by the follow up water was unstable (Table 6). The saturation of the flooding solution with PCE increased the viscosity and density of the mixture, which stabilized the displacement of resident water but destabilized the displacement of flooding solution by follow-up water.

The three-dimensional model was able to capture the displacement instability more accurately. The initial simulated breakthrough and the simulated plateau

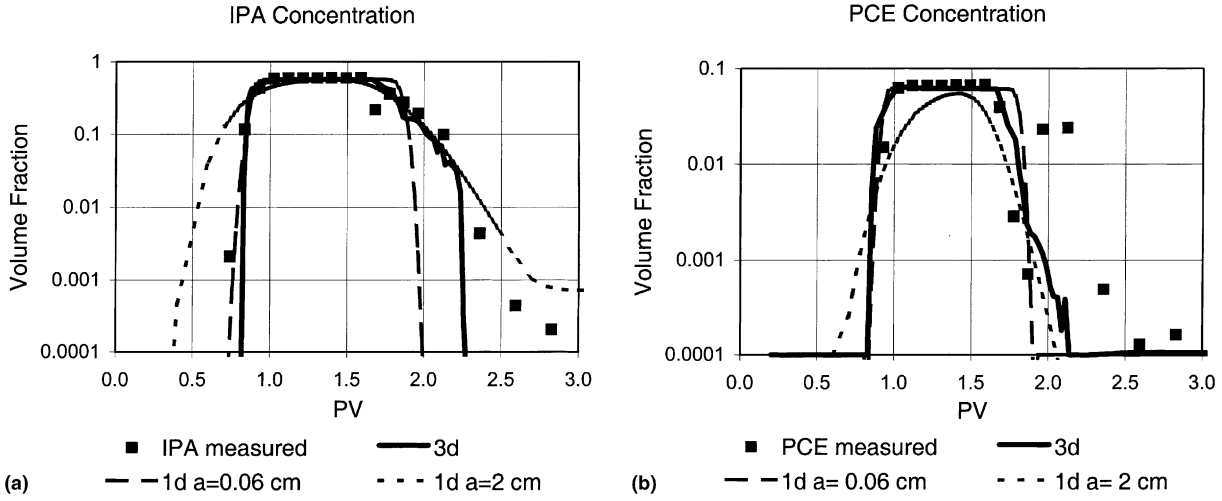

Fig. 4. The measured [9] and modeled effluent concentrations using a 60% IPA, 40% water flood in upward direction. (a) IPA (v/v), (b) PCE (v/v).

Table 6
Predicted stability for displacements during 60% IPA flood

Fluid 1 (displacing)	Fluid 2 (displaced)	v/v_{crit}	Stable if	Stability	ρ_1 (g/ml)	ρ_2 (g/ml)	μ_1 (mPa s)	μ_2 (mPa s)
PCE–saturated 60% IPA	Water	1.0	$v \geqslant v_{crit}$	Stable	0.938	0.998	3.43	0.95
Water	PCE–saturated 60% IPA	3.8	$v \leqslant v_{crit}$	Unstable	0.998	0.938	0.95	3.43

concentrations were nearly identical to the one-dimensional low-dispersivity simulation results. Most remarkable was the simulated earlier decrease in concentrations from the plateau compared to the low dispersivity one-dimensional simulations (Fig. 4). Contour plots for simulated IPA and PCE concentrations for three-dimensional simulations showed fingering to begin after the follow-up water reached the residual PCE in agreement with the stability consideration discussed above. The decrease in IPA due to water breakthrough was associated with a rapid decrease in PCE solubility. The long tailing of PCE concentrations in the simulation stemmed from production of PCE as separate phase. This production of PCE as a separate phase did not occur in the one-dimensional simulations discussed above [8,52], but was in agreement with Brandes' [9] experimental observations, where NAPL beads are mentioned. The layering of the bead pack resulted in layers of higher PCE saturations remaining. This phenomenon was also observed experimentally by Imhoff et al. [32].

The intermittent peak of PCE concentrations was not shown by any of the simulations. Brandes [9] suggested that this peak could have been caused by NAPL trapped in the effluent tubing. PCE, coming out of solution due to decreased alcohol concentrations in the upward directed effluent tubing, was not likely to flow into the sample container at the same velocity as the bulk aqueous phase due to the instability of displacement. The effluent tubing was not simulated in detail and thus some discrepancy between simulation and experiment could be accepted.

IPA concentrations decreased faster in the three-dimensional simulation than in the experiment. This could be due to partitioning of IPA out of the residual NAPL in the column into the aqueous phase, which was not simulated below a total concentration of 9% IPA. Final concentration were also reached later than modeled in the conservative tracer test attributed to bypassing effects [14,35].

Neglecting buoyancy forces in simulated capillary desaturation by using capillary numbers instead of total trapping number [18,46] resulted in simulated mobilization of some NAPL, which was not seen in the experiment. The density contrast between NAPL and flooding solution stabilized the NAPL under upward flooding conditions. The reduction in interfacial tension between flooding solution and NAPL to below 1 dynes/cm would result in mobilization during horizontal flooding at the same flow rate [46].

In summary, simulations of a column experiment utilizing enhanced dissolution showed agreement with the experimental data. For the injection rate of alcohol mixture into the column a discrepancy between modeled and reported experimental data was found, which may reflect uncertainties in influent configuration and reporting of the injection pressure. A three-dimensional simulation represented unstable displacement and provided a qualitatively better match of experimental effluent concentration data than the one-dimensional simulations. No fitting of parameters was necessary to achieve this improvement.

5.4. Separate phase mobilization

The NAPL can be mobilized as a separate phase due to swelling and reduction of interfacial tension. NAPL swelling occurs when an alcohol partitions out of the aqueous phase into the NAPL. The mobilizing experiments by Boyd [6], Brandes [9,10], and Milazzo [44] in the upward direction generally showed a NAPL bank that appeared simultaneously with increased alcohol concentrations in the effluent and continued for some time with the high alcohol concentrations. This was in contrast to fractional flow theory that would predict a DNAPL bank in the effluent before alcohol breaks through [21,48]. Previous simulations [8,52,55] of such separate phase mobilization experiments were in accordance with theory and predicted a well established NAPL bank in the effluent prior to alcohol breakthrough.

The transfer of alcohol from the aqueous phase to the NAPL can introduce mass transfer limitations into the process. Reitsma [52,55] found a more drawn out NAPL bank and significant tailing of alcohol for nonequilibrium simulations of a vertical upward displacement experiment using the water, *n*-propanol, TCE system. An alternative explanation for the later arrival and prolonged existence of the NAPL bank is a retardation of the bank, which is denser then the flooding solution, due to gravity instability and increased mixing.

Among Brandes' [9,10] glass bead column experiments involving separate phase displacements, the flooding of residual PCE with a 70% solution of TBA (experiment 2) was selected for simulation. The given effluent concentrations in mg/l [9] were converted to

volume fractions using the component densities. This experiment involved an alcohol strongly partitioning into the NAPL in contrast to the enhanced dissolution case discussed before. Brandes [9,10] investigated the partitioning behavior of this system. During the study by Roeder [57], viscosities and interfacial tensions of the ternary system were measured. Fluid properties are summarized in Table 7.

Fig. 5 compares the measured and simulated cumulative flows for several simulations. The given elevation gradient of 0.3 was too small to achieve continuous flow in one-dimensional simulations with medium dispersivity. The low dispersivity case was simulated by specifying the average flow rate during alcohol injection and without consideration of the glass frits. For the high dispersivity case, an increased gradient of 0.45 improved the agreement of flows. The three-dimensional simulation with this increased initial gradient showed for the first half pore volume similar flows as the high dispersivity case but had faster flow for the next pore volume. The final flow of water under a constant gradient was very similar in all three cases.

Reported and simulated effluent concentrations are compared in Fig. 6. In the one-dimensional simulation with low dispersivity and specified initial flow rate, the PCE-displacement was modeled as one bank before the TBA breakthrough. The TBA then followed undiluted. This behavior was also found in the simulations of this and similar cases by Brame [8] and Reitsma [52,55]. In contrast to this, the experiment showed TBA and PCE breakthrough simultaneously. The PCE concentrations in the experiment peaked later and broader. The tailing of the TBA concentrations was also not captured by the one-dimensional simulation.

Table 7
Fluid properties for the TBA/PCE/Water ternary system used in the simulation

Data at $T = 23°C$	
Hand parameters for phase behavior [9]	C^{n}_{pl}: 0.0141 (v/v)
	$B_n = B_w$: −1.14
	F: 6.04
C^{c}_{min}: 0.048	$C^{c}_{max'}$: 0.654 (v/v)
Interfacial tension	σ_0: 40 mN/m
X_0: −3.6	$k_{Li\ and\ Fu}$: 1.83
Density (g/ml) [39,56]	Density adjustments [39,57]
	$\rho_{w,TBA}$: 0.029
ρ_w: 0.998	$\rho_{TBA,w}$: 0.020
ρ_{PCE}: 1.62	$\rho_{PCE,TBA}$: −0.012
ρ_{TBA}: 0.783	$\rho_{TBA,PCE}$: −0.003
Viscosity (mPa s) [56]	Interaction parameter [57]
μ_w: 0.95	$d_{w,PCE}$: 7.14
μ_{PCE}: 0.87	$d_{w,TBA}$: 2.86
μ_{TBA}: 4.85	$d_{PCE,TBA}$: −2.16

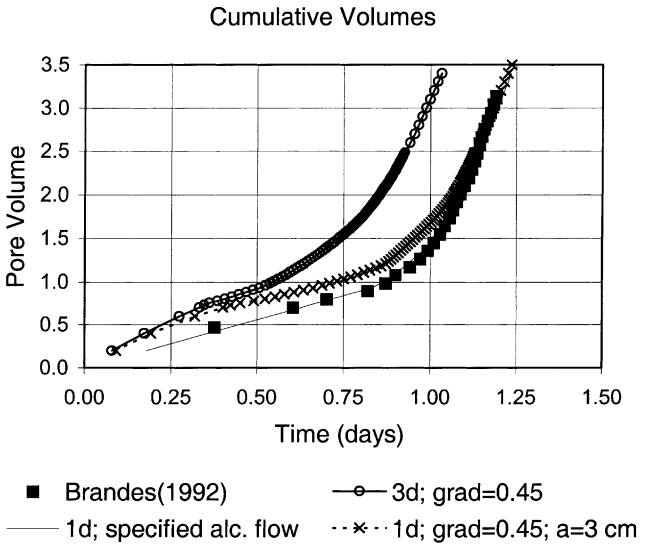

Fig. 5. Measured [9] and simulated cumulative pore volumes over time for 70% TBA flood.

Displacement of PCE by the flooding solution was expected to be very unstable (Table 8). The instability was expected to increase in the tubing, assumed to be 0.16 cm inner diameter. Displacement of flooding solution by follow-up water was also expected to be unstable.

The effluent concentrations of a one-dimensional simulation with increased dispersivity ($a = 3$ cm) are also shown in Fig. 6. The simulated TBA concentrations exhibited earlier breakthrough than measured. The decreased concentrations of the alcohol slug and the long tailing of TBA agreed fairly well (Fig. 6(a)). The high PCE concentrations of the NAPL bank extended further into the alcohol slug in this simulation. There was still a more pronounced DNAPL bank simulated than was observed. The shape of the bank remained the same in simulations that did not consider the glass frits separately or that increased NAPL relative permeability by reducing the NAPL relative permeability exponent from four to three. One plausible retarding influence for the DNAPL bank in the experiment was the effluent tubing. The DNAPL displaced initially out of the column may have remained in vertical effluent tubing until the density contrast with the aqueous phase and the mobility ratio were such that the critical velocity to displace the NAPL was exceeded. As in the case of the IPA/PCE experiment, a peak of NAPL was recovered at just over two pore volumes and not modeled in any simulation.

The TBA concentrations of the three-dimensional simulation agreed fairly well with the initial breakthrough and some of the tailing (Fig. 6(a)). The longer observed tailing of TBA concentrations compared to the simulation may have been due to TBA associated with the isolated peak of PCE concentrations and partitioning of TBA out of the NAPL that remained in the

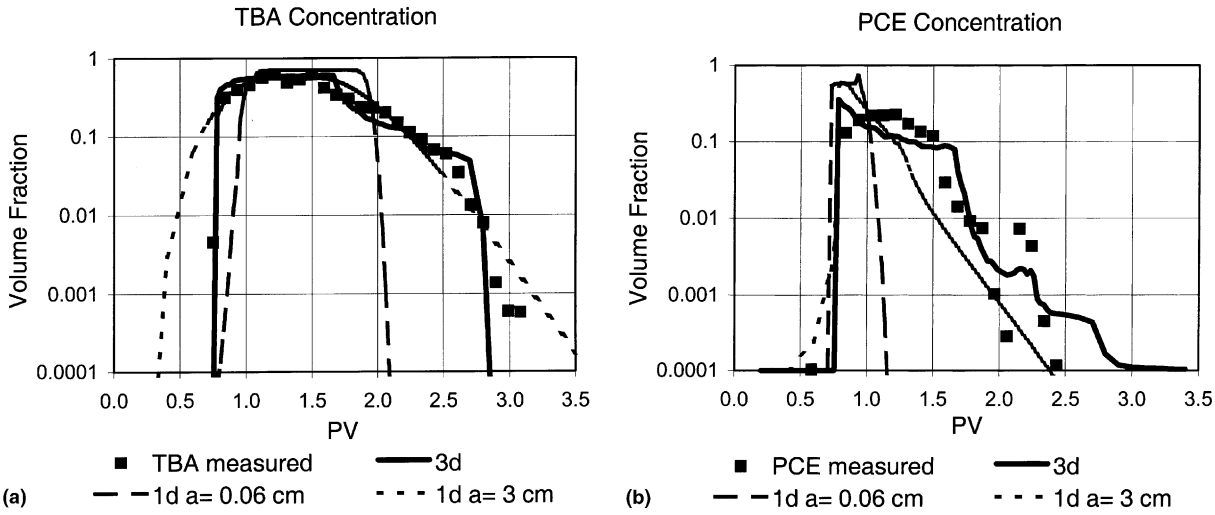

Fig. 6. The measured [9] and modeled TBA and PCE effluent concentrations using a 70% TBA, 30% water flood in upward direction. (a) TBA (v/v), (b) PCE (v/v).

Table 8
Predicted stability for displacements during 70% TBA flood

Fluid 1 (displacing)	Fluid 2 (displaced)	v/v_{crit}	Stable if	Stability	ρ_1 (g/ml)	ρ_2 (g/ml)	μ_1 (mPa s)	μ_2 (mPa s)
70% TBA	Water	1.2	$v \geqslant v_{crit}$	Stable	0.867	0.998	5.42	0.95
70% TBA	PCE	0.074	$v \geqslant v_{crit}$	Unstable	0.867	1.62	5.42	0.87
70% TBA	PCE in tubing	0.014	$v \geqslant v_{crit}$	Unstable	0.867	1.62	5.42	0.87
Water	70% TBA	2.1	$v \leqslant v_{crit}$	Unstable	0.998	0.867	0.95	5.42

column. The PCE bank in this simulation showed reduced concentration compared to one-dimensional simulations and extended further into the alcohol slug. The bank was still more pronounced in the simulation than observed.

5.5. Additive aided separate phase mobilization

As an example of a mobilizing alcohol flood involving two alcohols and to compare the results of a slightly varied experimental setup, experiment 2 reported by Milazzo [44] was simulated. In this experiment, the top glass frits had been removed and the effluent tubing had been shortened. In contrast to the experiments by Brandes [9,10], no spikes of NAPL component concentrations were observed in the effluent during the water flood. This observation is consistent with the influence of effluent tubing discussed above. The top two fifths of the column were contaminated with residual TCE. The column was then flooded with a mixture of 17% water, 67% *n*-butanol, and 16% methanol by volume at a constant rate of 430 ml/d in the upward direction. Only effluent concentration histories and no gradients were investigated because a gas phase appeared in the flooding solution during the experiment before it reached the NAPL [44]. Milazzo [44] explained this occurrence with a difference of gas solubility between resident water and flooding solution leading to gas coming out of solution at the interface. It was assumed that NAPL mobilization was not influenced by the gas phase, but that displacement of flooding solution by water was and therefore the water flooding part of the experiment was not considered in detail. The given effluent concentrations in mg/l [44] were converted to volume fractions using the component densities.

The Hand and interfacial tension parameters to describe phase behavior of the water, *n*-butanol, methanol, TCE systems were based on batch experiment measurements by Milazzo [44,57] and are given in Table 9. A comparison of two-phase effluent sample compositions with estimates using these parameters showed good agreement, supporting the equilibrium assumption. Samples with TCE concentrations of less than 0.05 v/v showed lower *n*-butanol concentrations in the NAPL than estimated. This discrepancy was as likely to be due to shortcomings of the phase behavior model than to nonequilibrium because the phase behavior characterization by Milazzo [44] did not include samples with such low TCE-concentrations. Estimated viscosity and density parameters are summarized in Table 10. Viscosity interactions were assumed to be the same as for TBA, water, and PCE. The methanol–water interaction parameter was determined from the viscosity data in Lide et al. [39]. The methanol–TCE interaction param-

Table 9
Phase behavior parameters used for simulations of the water, TCE, *n*-butanol, methanol quaternary system [44,57]

Feature of phase behavior		Parameter used in absence of additive		Influence of additive	
C^c_{min}	0.10	Symbol	Value	Slope parameter	Value
NAPL component concentration at plait point		$C^n_{pl,0}$	0.573E−4	$\Delta(1/C^n_{pl})/\Delta f^a_w$	34,664,000
Slope of tie-line line		F_0	5.586	$\Delta F/\Delta f^a_w$	1.72
Slope of NAPL solubility line		$B_{n,0}$	−2.054	$\alpha_n = \ln(B_n/B_{n,0})/\Delta f^a_w$	6.4
Intersection of aqueous solubility line with *y*-axis		$C^c_{max'}$	0.896	$\Delta(\log(A_w))/\Delta f^a_w$	17
Slope of aqueous solubility line		$B_{w,0}$	2.81	$\alpha_w = \ln(B_w/B_{w,0})/\Delta f^a_w$	1.43
Log of mutual solubilities		$X_{0,0}$	−2.92	$\Delta X_{0'}/\Delta f^a_w$	2.4
Li and Fu exponent		$k_{Li\ and\ Fu,0}$	1.78	$\Delta k_{Li\ and\ Fu}/\Delta f^a_w$	0.684
Aqueous solubility of TCE		Sol_0	0.0075		

Table 10
Densities and viscosity parameters used for simulations of the water, TCE, *n*-butanol, methanol quaternary system [44,57]

Data at $T = 22°C$	
Density (g/ml)	Density adjustments
	$\Delta\rho_{w,NBA}$: 0.029
ρ_w: 0.998	$\Delta\rho_{NBA,w}$: 0.020
ρ_{TCE}: 1.457	$\Delta\rho_{TCE,NBA}$: −0.012
ρ_{NBA}: 0.809	$\Delta\rho_{NBA,TCE}$: −0.003
ρ_{MeOH}: 0.789	$\Delta\rho_{w,MeOH}$: 0.019
	$\Delta\rho_{MeOH,w}$: 0.043
Viscosity (mPa s)	Interaction parameter
	$d_{w,TCE}$: 7.14
μ_w: 0.971	$d_{w,NBA}$: 2.86
μ_{TCE}: 0.553	$d_{TCE,NBA}$: −2.16
μ_{NBA}: 2.82	$d_{w,MeOH}$: 3.51
μ_{MeOH}: 0.576	$d_{TCE,MeOH}$: −0.375
	$d_{NBA,MeOH}$: 0

eter was assumed to be equal to the ethanol–PCE interaction parameter determined from data reported by Lunn [41].

Table 11 shows the expected stability of displacements. Again, the instability of the TCE displacement by the flooding solution was increased in the effluent tubing. According to these estimates the displacement of flooding solution by water should have been stable. Correspondingly there was little observed tailing for the alcohol concentrations beyond an initial offset which suggested a larger than simulated slug volume.

In Fig. 7 the effluent histories from the experiment are compared to the results of simulations. TCE concentrations in the experiment showed a bank followed by a plateau of lower concentrations before concentrations decreased after single-phase conditions were reached and recovery was complete. The one-dimensional simulation with low dispersivity showed a sharper NAPL bank than was observed. One-dimensional simulations with increased dispersivity showed a wider bank, which still did not account for the plateau of lower concentrations. A simulation using the three-dimensional column representation agreed with the fact of the prolonged recovery of TCE but indicated a less pronounced initial bank. In this simulation, recovery was not complete and therefore, TCE recovery continued throughout the simulation. The difference in bank formation suggested that the displacement was more stable than simulated, possibly due to an underestimation of mixture viscosities, for which no measurements had been available.

The step in observed alcohol concentrations at 1.4 PV stemmed from a step in *n*-butanol concentrations and was associated with the reaching of single phase conditions. A less pronounced and earlier step in alcohol concentrations was only modeled by the low dispersivity one-dimensional simulation but not by any of the other simulations (Fig. 7(a)).

The methanol breakthrough was simulated at lower initial concentrations than measured. An explanation for this was that the aqueous pseudocomponent in the NAPL phase was enriched in methanol compared to the aqueous phase according to the data by Milazzo [44]. The initially recovered NAPL thus had a higher

Table 11
Predicted stability for displacements during 67% *n*-butanol, 16% methanol flood

Fluid 1 (displacing)	Fluid 2 (displaced)	v/v_{crit}	Stable if	Stability	ρ_1 (g/ml)	ρ_2 (g/ml)	μ_1 (mPa s)	μ_2 (mPa s)
67% NBA/ 16% MeOH	Water	1.4	$v \geqslant v_{crit}$	Stable	0.849	0.998	2.71	0.970
67% NBA/ 16% MeOH	TCE	0.14	$v \geqslant v_{crit}$	Unstable	0.849	1.46	2.71	0.553
67% NBA/ 16% MeOH	TCE in tubing	0.029	$v \geqslant v_{crit}$	Unstable	0.849	1.46	2.71	0.553
Water	67% NBA/ 16% MeOH	0.66	$v \leqslant v_{crit}$	Stable	0.998	0.849	0.970	2.71

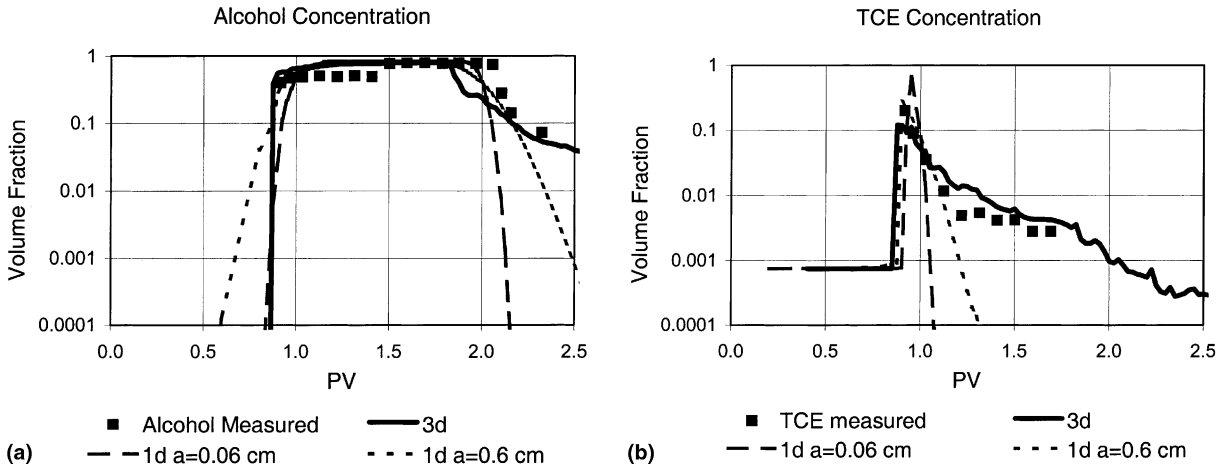

Fig. 7. Measured [44] and modeled TCE and alcohol effluent concentrations using a 67% *n*-butanol, 16% methanol, 17% water flood in upward direction. (a) total alcohol (v/v), (b) TCE (v/v).

methanol concentration than simulated. The pseudo-component approach of assuming equal methanol/water ratios in both phases would need to be modified to capture this behavior.

6. Discussion

Independently measured and estimated parameters resulted in reasonable matches of simulations to the experimental data. The equilibrium ternary and quaternary system descriptions chosen were sufficient to represent the vertical column experiments. Nonideal displacement that Reitsma and Kueper [55] had represented by assuming non-equilibrium was explained in the present study as the result of displacement instability. Of the column experiments discussed, only Milazzo [44] had analyzed the composition of two-phase samples to judge if equilibrium had been reached. The effluent data agreed well with the batch equilibrium phase behavior data provided by him. The phase behavior model deviated at high *n*-butanol, low TCE concentrations from the effluent concentrations because no batch experiments had been performed for these tie-lines and because the model did not represent the limited solubility of *n*-butanol in water.

Instability of displacement and dispersion result in a shortening of the effective alcohol slug volume [35,41,42,53]. The simulated experiments showed that the effect of this shortening depends on the type of alcohol flood. An enhanced dissolution flood, such as the IPA/PCE experiment by Brandes [9,10] reaches equilibrium between NAPL and flooding solution for as long as NAPL is present. An unstable displacement of the alcohol flood by water before all NAPL component has been recovered leads to precipitation as NAPL, which could only be simulated with a very fine mesh and not in one-dimensional simulations that used large dispersivities to model the mixing. Modeling the unstable displacement one-dimensionally with a large dispersivity lead to dilution of the alcohol slug and correspondingly lower predictions of NAPL component recovered (Table 12).

Mobilizing alcohol floods ideally displace the NAPL as a bank before the alcohol slug. The alcohol slug can therefore theoretically be shorter than in enhanced dissolution floods. In upward displacement of DNAPLs such as simulated here, the displacement of the bank by the alcohol slug is usually unstable. This instability and its impact on remediation effectiveness were seen in the three-dimensional simulations by a widening of the NAPL bank and incomplete recovery of the NAPL component (Table 12). Shorter slugs such as used in a different experiment by Milazzo [44], or in experiments by Lunn and Kueper [41,42] experienced also degradation of the NAPL bank, resulting in the formation of a residual swollen NAPL and a partitioning of the alcohol out of this NAPL back into the follow-up water. The

Table 12
Comparison of experimentally determined and simulated recoveries of NAPL component

Experiment	Measured removal	Simulated removal		
		One-dimensional	One-dimensional, large *a*	Three-dimensional
1 IPA/PCE	0.41	0.40	0.21	0.37
2 TBA/PCE	0.89	1.00	1.00	0.85
3 NBA/TCE	1.00	1.00	1.00	0.94

presented formulation of UTCHEM did not lend itself to simulation of this tailing because of the assumption that all alcohol below a given concentration is present in the aqueous phase.

The greater instability during the TBA/PCE experiment compared to the NBA/TCE experiment due to higher density contrast, lower flow rate and more effluent tubing resulted in a more spread out NAPL bank. One-dimensional simulations reflected this order by a lower matched effective dispersivity for the NBA/TCE simulation.

The displacement of alcohol by water was unstable for the case of IPA/PCE and TBA/PCE. This was accounted for by an apparent dispersivity two orders of magnitude larger than the medium dispersivity as determined by a conservative tracer test. Some tailing of alcohol at the end of the experiments was attributed to the effect of dead-end pores as also seen in the tracer experiment.

The displacement instabilities could be matched using a dispersivity that was adjusted to fit the extent of instability. This approach appears of limited usefulness for the general case. Mixing length as a measure of dispersion should grow with the square root of time but grows linearly or exponentially with time for unstable displacements [60,66]. Additionally, this approach is limited to one displacement. For displacements of several fluids by each other within one experiment, the several displacement fronts are likely to be subject to different displacement instabilities as was seen in the presented simulations for the displacement of water by alcohol and the displacement of alcohol by water.

Effluent tubing appeared to have an effect on the experimental results. In Brandes' [9,10] experiments, a peak of NAPL component was recovered at the tailing end of the alcohol slug, while this peak was absent in Milazzo's experiments [44] with shorter effluent tubing. Also, some of the difference between simulation and experiment for the initial PCE recovery in the TBE/PCE case could be caused by the effluent tubing in Brandes' case [9,10].

7. Conclusions

The adapted equilibrium multiphase compositional simulator using separately obtained phase behavior and porous medium property information matched the experimental data for several column experiments reasonably well. This agreement suggested that the equilibrium assumption was met in these experiments. Ternary and quaternary systems were simulated.

Displacement instability appeared to be the primary mechanism to explain deviations from ideal displacement in the experimental results. High-resolution three-dimensional simulations accounted for the effects of unstable displacement on NAPL component and alcohol recovery. An effective dispersivity approach was used to represent displacement instability in one-dimensional simulations.

This study indicated that particular attention should be paid to the characterization of stability for the design of alcohol flooding experiments. Simulations of unstable displacements require either high-resolution grids, or need to consider the mixing of fluids in a different manner to capture the resulting effects on NAPL recovery.

Acknowledgements

We thank Dr. Gary Pope and Dr. Mojdeh Delshad from the University of Texas at Austin for providing the source code of UTCHEM and for the training and suggestions received from them. We also appreciate the financial support of the US Environmental Protection Agency and the Westinghouse Savannah River Company and computing resources provided by the Institute of Environmental Engineering and Biotechnology at Tampere University of Technology in Finland during the revisions. This paper has not been subject to review by these agencies and does not necessarily reflect their views. The suggestions of four anonymous reviewers are gratefully acknowledged.

References

[1] Ace Glass. Catalog 1000. Vineland: Ace Glass; 1989.
[2] Amaefule JO, Handy LL. The effect of interfacial tensions on relative oil/water permeabilities of consolidated porous media. Soc Pet Eng J 1982;22:371–81.
[3] Bacri J-C, Rakotomala N, Salin D. Stable and unstable miscible flows through porous media. In: Banavar JR, Koplik J, Winkler KW, editors. Physics and chemistry of porous media II. AIP Conference Proceedings 154. New York: American Institute of Physics; 1987. p. 116–28.
[4] Bardon C, Longeron DG. Influence of very low interfacial tensions on relative permeability. Soc Pet Eng J 1980;20:391–401.
[5] Bergelin O, Lockhart FJ, Brown GG. Liquid–liquid extraction. Trans Amer Inst Chem Eng 1943;39:173–200.
[6] Boyd GR. Factors influencing nonaqueous phase liquid removal from groundwater by alcohol flooding. Ph.D. Dissertation, Department of Environmental Systems Engineering, Clemson University, Clemson, 1991.
[7] Boyd GR, Farley KJ. NAPL removal from groundwater by alcohol flooding, laboratory studies and applications. In: Calabrese EJ, Kostecki PT, editors. Hydrocarbon contaminated soils and groundwater, Vol. 2. Boca Raton: Lewis Publishers; 1992.
[8] Brame SE. Development of a numerical simulator for the in-situ remediation of dense nonaqueous phase liquids using alcohol flooding. M.S. thesis, Department of Geological Sciences, Clemson University, Clemson, 1993.
[9] Brandes D. Effect of phase behavior on residual dense nonaqueous phase liquid displacement from porous media by alcohol flooding. M.S. thesis, Department of Environmental Systems Engineering, Clemson University, Clemson, 1992.

[10] Brandes D, Farley KJ. Importance of phase behavior on the removal of residual DNAPLs from porous media by alcohol flooding. Water Environ Res 1994;65:869–78.
[11] Brown CL, Pope GA, Abriola LM, Sepehrnoori K. Simulation of surfactant-enhanced aquifer remediation. Water Resour Res 1994;30:2959–77.
[12] Camilleri D, Fil A, Pope GA, Rouse BA, Sepehrnoori K. Improvements in physical-property models used in micellar/polymer flooding. SPE Reserv Eng 1987;2(7):433–40.
[13] Chang S-H, Slattery JC. Nonlinear stability analysis of miscible displacements. Transp Porous Media 1990;5:49–69.
[14] Coats KH, Smith BD. Dead-end pore volume and dispersion in porous media. Soc Pet Eng J 1964;4:73–84.
[15] Corey AT. Mechanics of immiscible fluids in porous media. Highlands Ranch: Water Resources Publications; 1994.
[16] Coskuner G, Bentsen RG. An extended theory to predict the onset of viscous instabilities for miscible displacements in porous media. Transp Porous Media 1990;5:473–90.
[17] Datta Gupta A, Pope GA, Sepehrnoori K, King MJ. High resolution monotonic schemes for reservoir fluid flow simulation. In Situ 1991;15:289–317.
[18] Delshad M, Pope GA, Sepehrnoori K. A compositional simulator for modeling surfactant enhanced aquifer remediation. J Contam Hydrol 1996;23:303–28.
[19] Domenico PA, Schwartz FW. Physical and chemical hydrogeology. New York: Wiley; 1990.
[20] Falta RW. Program "Tracer", Implementation of the van Genuchten (1982) solution to one-dimensional tracer transport under the influence of dispersion, partitioning, and decay. Fortran Code. Clemson University, 10 August 1995.
[21] Falta RW. Using phase diagrams to predict the performance of cosolvent floods for NAPL remediation. Groundwater Monit Remed 1998;18:94–102.
[22] Finsterle S, Datta Gupta A. Siman. Program to compute stochastic fields using simulated annealing. Fortran Code. Lawrence Berkeley National Lab, 15 March 1996.
[23] Fountain JC. Technologies for dense nonaqueous phase liquid source zone remediation. Technology Evaluation Report TE-98-02. Groundwater Remediation Technologies Analysis Center, Pittsburgh, 1998.
[24] Gatlin C, Slobod RL. The alcohol slug process for increasing oil recovery. Trans AIME 1960;219:46–53.
[25] Gelhar LW, Axness CL. Three-dimensional stochastic analysis of macrodispersion in aquifers. Water Resour Res 1983;19:161–80.
[26] Grubb DG, Sitar N. Evaluation of technologies for in situ clean-up of DNAPL contaminated sites. Report EPA/600/R-94/120 August 1994. R.S. Kerr Environmental Research Laboratory US-EPA, Ada, 1994.
[27] Grunberg L, Nissan AH. Mixture law for viscosity. Nature 1949;164:799–800.
[28] Hand DB. Dineric distribution, I. The distribution of a consolute liquid between two immiscible liquids. J Phys Chem 1930; 34:1961–2000.
[29] Harmon TC, Kim T-J, Dela Barre BK, Chrysikopoulos CV. Cosolvent-water displacement in one-dimensional column. J Environ Eng 1999;125:87–91.
[30] Harten A. High resolution schemes for hyperbolic conservation laws. SIAM Rev 1983;25:35–67.
[31] Hornof V, Morrow NR. Gravity effects in the displacement of oil by surfactant solutions. SPE Reservoir Engineering November, 1987:627–33.
[32] Imhoff PT, Gleyzer SN, McBride JF, Vancho LA, Okuda I, Miller CT. Cosolvent-enhanced remediation of residual dense nonaqueous phase liquids, experimental investigation. Environ Sci Technol 1995;29:1966–76.
[33] Jawitz JW, Annable MD, Rao PSC. Miscible fluid displacement stability in unconfined porous media, two-dimensional flow experiments and simulations. J Contam Hydrol 1998;31: 211–30.
[34] Kueper BH, Frind EO. An overview of immiscible fingering in porous media. J Contam Hydrol 1988;2:95–110.
[35] Lake LW. Enhanced oil recovery. Englewood Cliffs, NJ: Prentice-Hall; 1989.
[36] Lenhard RJ, Parker JC, Mishra S. On the correspondence between Brooks–Corey and van Genuchten models. J Irrig Drain Eng 1989;115:744–51.
[37] Lenormand R. Statistical physics and immiscible displacements through porous media. AIP Conference Proceedings 154, Physics and Chemistry of Porous Media II; 1987. p. 98–115.
[38] Li B, Fu J. Interfacial tensions of two-liquid-phase ternary systems. J Chem Eng Data 1992;37:172–4.
[39] Lide DR. CRC handbook of chemistry and physics. 77 ed. Boca Raton: CRC Press; 1996.
[40] Liu J, Delshad M, Pope GA, Sepehrnoori K. Application of higher-order flux-limited methods in compositional simulation. Transp Porous Media 1994;16:1–29.
[41] Lunn SRD. Alcohol Flooding of porous media contaminated with hazardous immiscible liquids. Ph.D. dissertation, Department of Civil Engineering, Queen's University, Kingston, 1998.
[42] Lunn SRD, Kueper BH. Risk reduction during chemical flooding: preconditioning DNAPL density in situ prior to recovery by miscible displacement. Environ Sci Technol 1999;33:1703–8.
[43] Luthy RG, Dzombak DA, Peters C, Ali MA, Roy SB. Solvent extraction for remediation of manufactured gas plant sites. Final Report No. EPRI TR-101845 to the Electric Power Research Institute, Palo Alto, 1992.
[44] Milazzo JT. Remediation of DNAPL-contaminated groundwater using alcohol flooding, separate phase displacement vs. enhanced dissolution. M.S. thesis, Department of Environmental Systems Engineering, Clemson University, Clemson, 1993.
[45] Moissis DE, Wheeler MF, Miller CA. Simulation of miscible viscous fingering using a modified method of characteristics: effects of gravity and heterogeneity. SPE Adv Technol Ser 1993;1:62–70.
[46] Pennell KD, Pope GA, Abriola LM. Influence of viscous and buoyancy forces on the mobilization of residual Tetrachloroethylene during surfactant flushing. Environ Sci Technol 1996;30:1328–35.
[47] Pope GA, Nelson RC. A chemical flooding compositional simulator. Soc Pet Eng J 1978;18:339–54.
[48] Pope GA. The application of fractional flow theory to enhanced oil recovery. Soc Pet Eng J, Trans AIME 1980;268:191–205.
[49] Provoust LG, Pope GA, Rouse BA. Microemulsion phase behavior, a thermodynamic modeling of the phase partitioning of amphiphilic species. Soc Pet Eng J 1985;25:693–703.
[50] Pruess K. A Fickian diffusion model for the spreading of liquid plumes infiltrating in heterogeneous media. Transp Porous Media 1996;24:1–33.
[51] Reid RC, Prausnitz JM, Poling BE. The properties of gases and liquids. New York: McGraw-Hill; 1987.
[52] Reitsma S. Equilibrium and non-equilibrium compositional alcohol flooding models for recovery of immiscible liquids from porous media. Ph.D. Dissertation, Department of Civil Engineering, Queen's University, Kingston, 1996.
[53] Reitsma S, Kueper BH. Compositional modeling study of alcohol flooding for recovery of DNAPL. In: Reddi LN, editor. Non-aqueous phase liquids (NAPLS) in subsurface environment, assessment and remediation. New York: ASCE; 1996. p. 526–37.
[54] Reitsma S, Kueper BH. Non-equilibrium alcohol flooding model for immiscible phase remediation: 1. Equation development. Adv Water Resour 1998;21:649–62.
[55] Reitsma S, Kueper BH. Non-equilibrium alcohol flooding model for immiscible phase remediation: 2. Model development and application. Adv Water Resour 1998;21:663–78.

[56] Riddick JA, Bunger WB, Sakano TK. Organic solvents; physical properties and methods of purification, vol. 2. 4th ed. Techniques of Chemistry Series. New York: Wiley; 1986.
[57] Roeder E. Phase density modifications for the remediation of DNAPLS by cosolvent flooding utilizing separate phase mobilization. Ph.D. dissertation. Department of Environmental Systems Engineering. Clemson: Clemson University; 1998.
[58] Satoh T. Treatment of phase behavior and associated properties used in a micellar-polymer flood simulator. M.S. thesis, The University of Texas, Austin, TX, 1984.
[59] Slobod RL, Howlett WE. The effects of gravity segregation in laboratory studies of miscible displacement in vertical unconsolidated porous media. Trans AIME 1964;231:1–8.
[60] Tan CT, Homsy GM. Stability of miscible displacements in porous media: rectilinear flow. Phys Fluids 1986;29: 3549–56.
[61] Tan CT, Homsy GM. Simulation of nonlinear viscous fingering in miscible displacement. Phys Fluids 1988;31:1330–8.
[62] Treybal RE, Weber LD, Daley JF. The system acetone–water–1,1,2-trichloroethane. Ind Eng Chem 1946;38:817–21.
[63] van Genuchten MT. A closed-form equation for predicting the hydraulic conductivity of unsaturated soils. Soil Sci Soc Am J 1980;44:892–8.
[64] van Genuchten MT, Alves WJ. Analytical solutions of the one-dimensional convective–dispersive solute transport equation. Agricultural Research Service, US Department of Agriculture, Washington, DC, 1982.
[65] Wang Z, Feyen J, Elrick DE. Prediction of fingering in porous media. Water Resour Res 1998;34:2183–90.
[66] Welty C, Gelhar LW. Stochastic analysis of the effects of fluid density and viscosity variability on macrodispersion in heterogeneous porous media. Water Resour Res 1991;27:2061–75.